Journal of Interdisciplinary Mathematics
ISSN: 0972-0502 (Print), ISSN: 2169-012X (Online)
Vol. 29 (2026), No. 4, pp. 891–908
DOI : 10.47974/JIM-2346

Influence of shape factor on the tangent hyperbolic hybrid nanofluid flow over a nonlinear stretching sheet with Cattaneo-Christov heat flux : An irreversibility analysis

Vembakam Manjula *
R. Bhuvana Vijaya †
Department of Mathematics
JNTUA College of Engineering
Ananthapuramu 515002
Andhra Pradesh
India

Abstract

The aim of this work is to investigate the movement of the tangent hyperbolic hybrid nanofluid across a nonlinear elastic surface under the influence of various parameters including thermal radiation and magnetic field. The principal equations of the present problem have been turned into a collection of ordinary differential equations using the appropriate similarity transformations. Then, the bvp4c solver is used to resolve them. Multiple linear regression is used to analyze engineering parameters like the friction factor. Results are shown for both spherical and platelet-shaped nanoparticles. It is shown that an increase in the volume fraction of graphene oxide nanoparticles correlates with an enhancement in the heat transfer rate. It has been found that a stronger magnetic field and more nanoparticles slow down the flow of fluid. An upsurge in the couple stress parameter is found to result in an upsurge in the creation of entropy. We find that for both cases, the friction factor increases by 7.69% as the couple stress parameter value falls between 0.5 and 3 while the rate of heat transfer rises by 19.83% for spherical nanoparticles and 18.74% for platelet nanoparticles when the thermal radiation parameter values fall between 0 to 2.5.

Subject Classification: *76A05, 76Dxx, 76W05, 76R10.*

Keywords: *Non-Newtonian fluid, bvp4c, Magnetic field, Couple stress, Weissenberg number.*

* *E-mail:* **manjula418@gmail.com (Corresponding Author)**
† *E-mail:* **bhuvanarachamalla.maths@jntua.ac.in**

© Taru Publications

1. Introduction

Nanofluids and hybrid nanofluids hold immense significance due to their enhanced thermal properties. These engineered fluids, comprising nanoparticles dispersed in a base fluid, revolutionize heat transmission applications. When related to traditional fluids, nanofluids made of a single nanoparticle type have superior thermal conductivity and transfer of heat factors. Hybrid nanofluids, incorporating multiple nanoparticle types, further amplify these benefits, leading to superior thermal performance. Their applications span diverse industries, including electronics cooling, automotive, aerospace, and renewable energy. By enabling efficient heat dissipation, these fluids contribute to energy conservation, improved system performance, and advancements in various technological domains. Using a shooting approach, Pourmehran, Gorji, and Ganji [1] examined the convective movement of several nanofluids over a vertically stretched sheet heated by radiation. As the volume percentage of nanoparticles surges, a decline in the friction factor is noted. Afify [2] investigated the dynamics of a chemically reactive non-Newtonian nanofluid across an elastic sheet, incorporating viscous dissipation. Seth et al. [3] explored the movement of nanofluid through a permeable nonlinear elastic sheet in the slip regime. Rasool et al. [4] analyzed the non-Darcy movement of a nanofluid incorporating the Brownian motion parameter by the homotopy analysis approach, maintaining the same geometry. A correlation exists between the increase in the Brownian motion parameter and the concentration of the nanofluid. Misra and Kamatam [5] examined the magnetohydrodynamic movement of a nanofluid across an elastic surface within a slip regime. Kumar et al. [6] explored the radiative and chemically reactive transport of a nanofluid within the identical geometry utilizing the KKL nanofluid framework. An increase in the Biot number correlates with a rise in the fluid's temperature. Subsequently, different authors [7-8] examined diverse non-Newtonian nanofluid movements through a stretchy surface. Shah et al. [9] used the RKF-45 approach to analyse the chemical reaction-induced movement of a hybrid nanofluid across an elastic sheet. Farooq et al. [10] explored the movement of a hybrid nanofluid containing engine oil across a spinning sheet in the presence of a magnetic field and heat source settings. An upsurge in the heat source parameter is associated with an escalation in fluid temperature. Patil, Goudar, and Sheremet [11] inspected the periodic magnetohydrodynamic motion of a non-Newtonian nanofluid within a cylindrical structure. In their study, Mohana and Kumar [12] investigated

how form parameters affect the viscous dissipation parameter during the unstable transfer of a non-Darcy hybrid nanofluid through an elastic sheet. Later, different authors [13-14] examined diverse hybrid nanofluid movements through a stretchy surface with various parameters including cross-diffusion effects.

Entropy generation optimization in fluid flow is a powerful tool for improving the efficiency and performance of various engineering systems. By minimizing the rate of entropy production, we can reduce energy losses due to irreversibilities like friction and heat transfer. This optimization technique finds applications in diverse fields, including heat exchangers, power plants, and microfluidic devices. It helps in designing systems with lower energy consumption, reduced environmental impact, and enhanced overall efficiency. Jamshed and Aziz [15] investigated the optimization of the production of entropy in the movement of non-Newtonian hybrid nanofluid utilizing a non-Fourier heat flux framework. A surge in the unsteady parameter correlates with an upsurge in entropy creation. Mahdy [16] examined the influence of relevant parameters on entropy formation in the movement of tangent hyperbolic nanofluid via an upright cylindrical channel utilizing the Keller-Box method. A surge in the volume percentage of nanoparticles correlates with a rise in entropy generation. Hanif, Khan, and Shafie [17] conducted an irreversibility investigation of the magnetohydrodynamic hybrid nanofluid movement through an upright cone. Alazwari, Abu-Hamdeh, and Goodarzi [18] studied the optimization of entropy generation in the movement of viscoelastic nanofluids via the Keller-Box approach. The system's entropy influences the values of several factors, including suction and material properties. Kayalvizhi and Kumar [19] investigated the entropy generation rate in the movement of aqueous hybrid nanofluid through an elastic sheet and discovered a fall in the Bejan number with a spike in the magnetic field parameter. After that, many authors [20-22] conducted irreversibility investigations for distinct fluid flows via multiple geometries with varying parameters.

Tangent hyperbolic hybrid nanofluids have several practical uses owing to their superior thermal conductivity and heat transfer characteristics. Their flow over nonlinear stretching sheets is particularly relevant in industries like manufacturing, metallurgy, and electronics. While a little research has been performed on the movement of tangent hyperbolic hybrid nanofluid across diverse geometries, the specific case of a nonlinear elastic surface, coupled with the impact of magnetic field, shape factor, non-Fourier heat flux, and other physical parameters, offers

unique challenges and opportunities. The objective of this work is to examine the intricate interplay of these parameters on the movement and heat transmission characteristics of the tangent hyperbolic hybrid nanofluid. We intend to quantify the influence of numerous physical characteristics on important performance indicators, including skin friction coefficient, by multiple linear regression analysis.

2. Formulation of the Study

This research looks at the steady movement of tangent hyperbolic hybrid nanofluid through a nonlinear elastic sheet with non-Fourier heat flux and how several parameters, such as shape factor and couple stress, affect it. In this investigation, we presuppose the following:

(i) Please refer to Table 1 for the precise estimates of the thermo-physical features of EG, GO, and MWCNT

(ii) A vertically imposed external magnetic field of strength B affects the flow (see Figure 1).

(iii) This investigation excludes the influence of the induced magnetic field and viscous dissipation.

The subsequent circumstances and equations are requisite for this study, predicated on the aforementioned assumptions [23-24]:

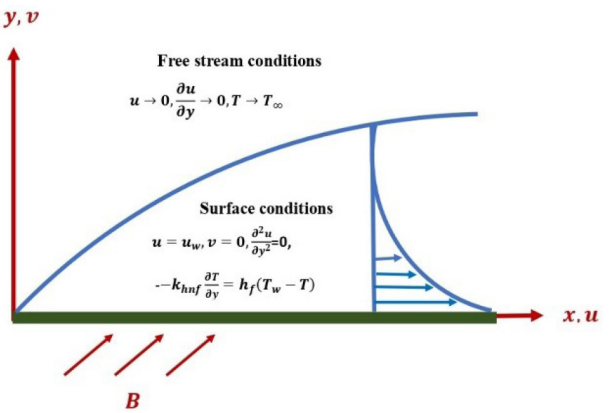

Figure 1

Diagrammatical representation of the present study

$$\frac{\partial v}{\partial y}+\frac{\partial u}{\partial x}=0, \tag{1}$$

$$u\frac{\partial u}{\partial x}+v\frac{\partial u}{\partial y}=(1-n)\frac{\mu_{hnf}}{\rho_{hnf}}\frac{\partial^2 u}{\partial y^2}+\sqrt{2}n\frac{\mu_{hnf}}{\rho_{hnf}}\Upsilon\left(\frac{\partial u}{\partial y}\right)\frac{\partial^2 u}{\partial y^2}-\frac{\sigma_{hnf}}{\rho_{hnf}}uB^2 -\frac{1}{\rho_{hnf}}\gamma_0\frac{\partial^4 u}{\partial y^4}, \tag{2}$$

$$v\frac{\partial T}{\partial y}+u\frac{\partial T}{\partial x}=\left(\left(k_{hnf}+\frac{16}{3}\frac{\sigma^* T_\infty^3}{k^*}\right)\frac{\partial^2 T}{\partial y^2}\right)\frac{1}{(\rho C_p)_{hnf}} -\delta\left[\begin{array}{l} u^2\frac{\partial^2 T}{\partial x^2}++2uv\frac{\partial^2 T}{\partial x\partial y}\frac{\partial T}{\partial x}+v^2\frac{\partial^2 T}{\partial y^2}+ \\ u\frac{\partial T}{\partial x}\frac{\partial u}{\partial x}+v\frac{\partial T}{\partial x}\frac{\partial u}{\partial y}+u\frac{\partial T}{\partial y}\frac{\partial v}{\partial x}+v\frac{\partial T}{\partial y}\frac{\partial v}{\partial y} \end{array}\right], \tag{3}$$

$$\left.\begin{array}{l} \text{at } y=0: u=u_w=bx^m, \frac{\partial^2 u}{\partial y^2}=0, v=0, \\ \frac{\partial T}{\partial y}k_{hnf}=(T-T_w)h_f, \\ \text{as y}\to\infty: T\to T_\infty, \frac{\partial u}{\partial y}\to 0, u\to 0. \end{array}\right\} \tag{4}$$

For the purpose of converting governing equations, Algehyne et al. [25] introduced the following similarity transformations:

$$\left.\begin{array}{l} \eta=yx^{\frac{m-1}{2}}\sqrt{\frac{b(m+1)}{2\upsilon}}, u=bx^m f'(\eta), \\ v=-\left[\eta\left(\frac{m-1}{m+1}\right)f'(\eta)+f(\eta)\right]\sqrt{\frac{b\upsilon(m+1)}{2}}x^{\frac{m-1}{2}}, \\ T=T_\infty+(T_w-T_\infty)\theta(\eta). \end{array}\right\} \tag{5}$$

Equation (1) can be readily satisfied by the terms presented in (5). The successful modification of equations (2-3) and conditions in (4) through integration of (5) yields the following result:

$$\frac{1}{S_1 S_2}\frac{m+1}{2}(1-n)f'''+\frac{1}{S_1 S_2}\frac{m+1}{2}nWef''f'''$$
$$-\frac{S_3}{S_1}Mgf'-\left(\frac{m+1}{2}\right)^2\frac{1}{S_1}Csf^{v}+\frac{m+1}{2}ff''-mf'^2=0, \tag{6}$$

$$\frac{m+1}{2}\left(\frac{S_4}{S_5}+\frac{Ra}{S_5}\right)\frac{1}{\Pr}\theta''-\Gamma\left(\frac{m+1}{2}\right)\left(\frac{m+1}{2}\right)f^2\theta''+\frac{1}{2}(m+1)f\theta'$$
$$+\Gamma\left(\frac{m^2-1}{4}ff'\theta'+\left(\frac{m-1}{2}\right)\left(\frac{m-1}{2}\right)\eta^2 f'^2\theta'^2\right)=0, \tag{7}$$

$$\left.\begin{aligned} &f(\eta)\big|_{\eta=0}=0,\theta'(\eta)\big|_{\eta=0}=-\frac{1}{S_4}(1-\theta(\eta))Bi\Big|_{\eta=0},\\ &f'(\eta)\big|_{\eta=0}=1,f'''(\eta)=0,\\ &f'(\eta)\big|_{\eta\to\infty}\to 0,\theta(\eta)\big|_{\eta\to\infty}\to 0,f''(\eta)\big|_{\eta\to\infty}\to 0. \end{aligned}\right\} \tag{8}$$

Here

$$\left.\begin{aligned} &\Gamma=\delta_0 b,\delta_0=\delta x^{m-1},Mg=\frac{\sigma_f B_0^2}{\rho b},B=B_0 x^{\frac{m-1}{2}},\\ &We=\Upsilon_0\sqrt{\frac{(m+1)bu_w^2}{2\upsilon}},\\ &\Upsilon_0=\Upsilon x^{\frac{m-1}{2}},Cs=\frac{\gamma_1 b}{\rho\upsilon^2},\gamma_1=\gamma_0 x^{m-1},Ra=\frac{16}{3}\frac{\sigma^* T_\infty^3}{kk^*},\\ &\Pr=\frac{\mu C_p}{k},Bi=\frac{a}{k_f\sqrt{\frac{b(m+1)}{2\upsilon}}},h_f=ax^{\frac{m-1}{2}}, \end{aligned}\right\}$$

and

$$
\left.
\begin{aligned}
S_5 &= (1-\phi_M)\left[(1-\phi_G)+\phi_G\frac{(\rho C_p)_G}{(\rho C_p)_f}\right]+\phi_M\frac{(\rho C_p)_M}{(\rho C_p)_f},\\
S_{31} &= \frac{\sigma_G+2\sigma_f-2\phi_G(\sigma_f-\sigma_G)}{\sigma_G+2\sigma_f+\phi_G(\sigma_f-\sigma_G)}, S_2=((1-\phi_G)(1-\phi_M))^{2.5},\\
S_1 &= \phi_M\frac{\rho_M}{\rho_f}+(1-\phi_M)\left[(1-\phi_G)+\phi_G\frac{\rho_G}{\rho_f}\right],\\
S_4 &= S_{41}\times\frac{k_M-2\phi_M(S_{41}k_f-k_M)+2S_{41}k_f}{k_M+\phi_M(S_{41}k_f-k_M)+2S_{41}k_f},\\
S_3 &= S_{31}\times\frac{\sigma_T+2S_{31}\sigma_f-2\phi_M(S_{31}\sigma_f-\sigma_M)}{\sigma_T+2S_{31}\sigma_f+\phi_M(S_{31}\sigma_f-\sigma_M)},\\
S_{41} &= \frac{k_G-2\phi_G(k_f-k_G)+2k_f}{k_G+\phi_G(k_f-k_G)+2k_f}.
\end{aligned}
\right\}
$$

Table 1

Key parameters' values of *EG*, *GO*, and *MWCNT* Prashar and Ojjela [26]

Properties	*EG* (f)	*GO* (f_G)	*MWCNT* (f_M)
$\sigma(Sm^{-1})$	1.10×10^{-4}	6.30×10^{7}	0.00019
$k(Wm^{-1}K^{-1})$	0.253	5000	3000
$\rho(kgm^{-3})$	1115	1800	2100
$C_p(Jkg^{-1}K^{-1})$	2430	717	711

The equation for the friction factor is as follows:

$$Cf=\frac{2}{\rho}\left(\frac{\partial u}{\partial y}\right)\frac{\mu_{hnf}}{u_w^{\,2}}\bigg|_{y=0}. \tag{9}$$

Utilizing (5) allows for a simplified formulation of the formula used in equation (9) as:

$$\sqrt{\mathrm{Re}_x}Cf = \sqrt{2(m+1)}\frac{1}{S_2}f''(0).$$

To figure out the heat transmission rate, one can utilize the subsequent approach:

$$Nu = \frac{-x\left(k_{hnf} + \frac{4}{3}\frac{4\sigma^* T_\infty^3}{k^*}\right)}{k_f(T_w - T_\infty)}\left.\frac{\partial T}{\partial y}\right|_{y=0}. \tag{10}$$

By employing (5), the formula utilized in (10) can be succinctly reformulated as:

$$(\mathrm{Re}_x)^{-1/2}Nu = -\sqrt{\frac{m+1}{2}}(S_4 + Ra)\theta'(0).$$

2.1 *Irreversibility formulation*

The formula that expresses the dimensional calculation of entropy generation as follows:

$$S_g = \left(\frac{k_f}{T_\infty^2}\right)\left(\frac{k_{hnf}}{k_f} + 16\frac{\sigma^* T_\infty^3}{3k_f k^*}\right)\left(\frac{\partial T}{\partial y}\right)^2 + \frac{\mu_{hnf}}{T_\infty}\left(\frac{\partial u}{\partial y}\right)^2 + \frac{\sigma_{hnf}}{T_\infty}u^2B^2. \tag{11}$$

By adopting (5), we may rewrite equation (11) as follows:

$$N_{EG} = \frac{m+1}{2}(S_4 + Ra)\alpha\theta'^2 + \frac{m+1}{2}\frac{Br}{S_2}f''^2 + S_3 Brf'^2\, Mg, \tag{12}$$

where

$$Br = \frac{\mu_f u_w{}^2}{(T_w - T_\infty)k_f}, N_{EG} = \frac{\upsilon T_\infty S_g}{bx^{m-1}(T_w - T_\infty)k_f}.$$

The Bejan number can be estimated by adopting the subsequent procedure:

$$Be = \frac{\text{Entropy formation due to the transfer of heat}}{\text{The overall generation of entropy}}.$$

Applying (12) in the following way allows us to revise *Be* :

$$Be = \frac{\frac{m+1}{2}(S_4 + Ra)\alpha\theta'^2}{\frac{m+1}{2}(S_4 + Ra)\alpha\theta'^2 + \frac{m+1}{2}\frac{Br}{S_2}f''^2 + S_3 Brf'^2 Mg}.$$

3. Numerical Procedure

The in-built function bvp4c in MATLAB is employed to resolve equations (6-7) with the constraints (8). This function effectively handles the given conditions (8) to provide accurate solutions. bvp4c implements a finite difference method based on the Lobatto IIIa formula. This method is known for its efficiency in terms of computational cost. Additionally, it's a robust solver, meaning it can handle a wide range of BVPs without encountering stability issues as often compared to some other techniques. Boundary value problems need to be well-posed for any numerical solver to find a unique and stable solution. bvp4c won't be able to determine if a problem is ill-posed (missing information or has multiple solutions), and it might struggle to converge in such cases. We conduct a comparative analysis of our findings with previously published data obtained under comparable conditions to authenticate their reliability. According to the statistics in Table 2, there is a high level of agreement.

Table 2

Validation of the present results for skin friction coefficient

M	Akbar, Ebaid, and Khan [27]	Amer et al. [28]	Present results
0	1.000000	1.0000000000	1.000008021
1	1.414210	1.4138890125	1.414213563
5	2.449449	2.4497898903	2.44948974
10	3.316630	3.3169899072	3.316624791

4. Results and discussion

4.1 *Velocity and temperature profiles*

In this study, it is assumed that $0 \le W_e \le 0.7$, $0 \le \Gamma \le 0.3$, $0 \le Ra \le 2$, $0 \le \phi_G \le 0.1$, $0.5 \le Cs \le 3$, $0 \le Mg \le 3$, $0.1 \le Br \le 1.5$, $0.1 \le Bi \le 0.5$. As Weissenberg number increases, the fluid transitions from Newtonian to shear-thickening behaviour. This means the fluid's viscosity surges with

shear rate. Consequently, the fluid experiences greater resistance to flow, leading to a decrease in velocity (see Figure 2). An augmentation in the couple stress parameter results in a reduction of the fluid's viscosity, hence diminishing its resistance to flow. This diminished resistance facilitates the fluid's flow, leading to an enhancement in its velocity (see Figure 3). An augmentation of the magnetic field parameter leads to an intensified Lorentz force exerted on the electrically conductive fluid. This force counteracts the fluid's velocity, hence augmenting the resistance to flow. Consequently, the fluid's velocity diminishes (see Figure 4). Thermal relaxation time refers to the average time it takes for a fluid particle to transfer its thermal energy to its surroundings. With a longer relaxation time, the particles have more time between collisions. This allows them to distribute their thermal energy more slowly. This causes the fluid's temperature to drop (see Figure 5). An increase in ϕ_G leads to a higher thermal conductivity of the fluid. This enhanced thermal conductivity allows for more efficient heat transfer, resulting in a higher fluid temperature. Additionally, the increased number of nanoparticles can lead to greater absorption of heat energy, further contributing to the temperature rise (see Figure 6).

The escalation of thermal radiation results in a temperature elevation of a fluid, since thermal radiation conveys energy via electromagnetic waves from a hotter surface or environment to the fluid. When the fluid absorbs this radiation, the energy stimulates its molecules, elevating their kinetic energy. This molecular agitation results in an increase in the fluid's temperature (see Figure 7).

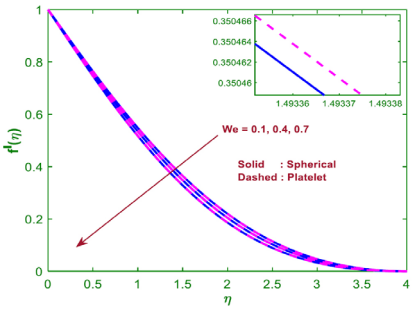

Figure 2

Influence of Weissenberg number on velocity profile

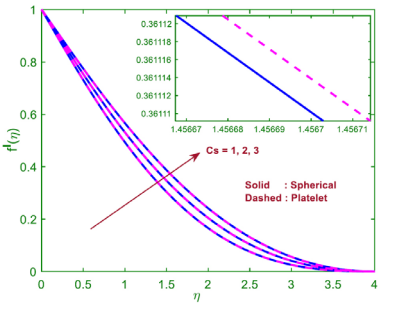

Figure 3

Influence of couple stress parameter on velocity profile

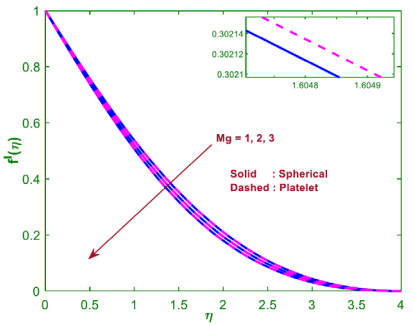

Figure 4

Influence of magnetic field parameter on velocity profile

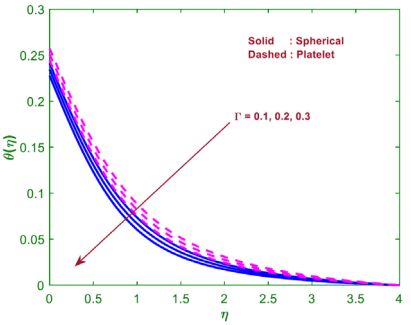

Figure 5

Influence of thermal relaxation parameter on temperature profile

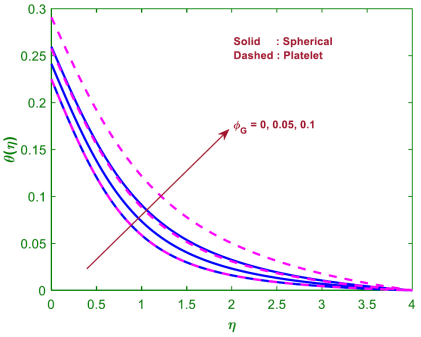

Figure 6

Influence of volume fraction of graphene oxide nanoparticles on temperature profile

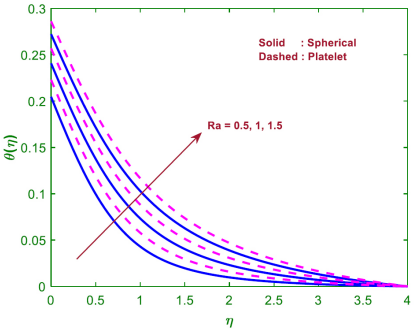

Figure 7

Influence of thermal radiation on temperature profile

4.2 *Irreversibility Analysis*

As the Brinkman number upsurges, the entropy generation surges and the Bejan number declines, as shown in Figures 8 and 9. A surge in Br indicates a larger contribution of viscous dissipation to the overall energy balance. This leads to increased frictional heating within the fluid, causing a higher temperature gradient. Consequently, the rate of heat transmission and the formation of entropy escalate. Figures 10–11 show that the upsurge in *Cs* causes a decline in the Bejan number profile and a surge in the entropy profile. An upsurge in the couple stress parameter enhances fluid

flow velocity, which, in turn, leads to increased fluid friction. This increased friction dissipates more kinetic energy into thermal energy, resulting in a higher temperature gradient within the fluid. Consequently, the rate of entropy generation rises due to both the increased fluid friction and the enhanced thermal gradients.

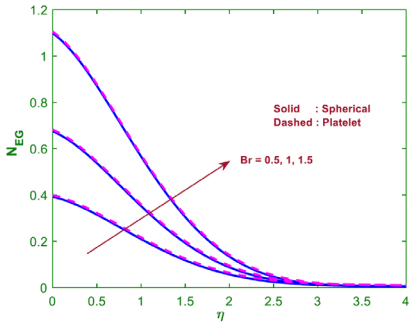

Figure 8

Influence of Brinkman number on entropy generation profile

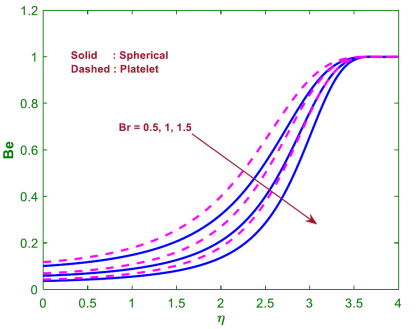

Figure 9

Influence of Brinkman number on Bejan number profile

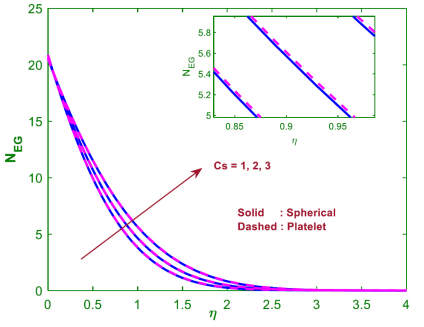

Figure 10

Influence of couple stress parameter on entropy generation profile

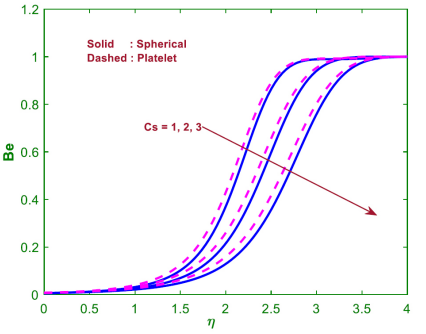

Figure 11

Influence of couple stress parameter on Bejan number profile

4.3 *Multiple linear regression*

By utilizing the models provided below, this study established a connection between crucial technical qualities, like the friction factor, and specific variables, like the couple stress parameter:

$$Cf = p_0 + p_1 Cs + p_2 Mg \tag{13}$$

$$Nu = q_0 + q_1 Ra + q_2 \phi_G \tag{14}$$

We used 20 different sets of variables for each computation to speed up the process of discovering results:

$$Cf = -0.5652 - 0.1341 Cs + 0.289 Mg \tag{15}$$

$$Nu = 0.3144 + 0.1974 Ra + 0.6581 \phi_G \tag{16}$$

According to equation (15), the friction coefficient declines as Cs surge, but it upsurges as Mg surges. An upsurge in the couple stress parameter reduces the skin friction coefficient because it decreases the fluid's viscosity. This reduction in viscosity leads to a decrease in the shear stress at the surface, resulting in a lower skin friction coefficient. We find that for both cases, the friction factor increases by 7.69% as the couple stress parameter value falls between 0.5 and 3. According to equation (16), the Nusselt number upsurges as *Ra* and ϕ_G surges. When thermal radiation increases, more heat energy is transferred from the fluid to the surrounding environment through electromagnetic waves. This additional heat transfer mechanism supplements the existing convective and conductive heat transfer, resulting in a higher overall heat transfer rate. Since the Nusselt number is directly proportional to the heat transfer rate, an increase in thermal radiation ultimately leads to a higher Nusselt number. The rate of heat transfer rises by 19.83% for spherical nanoparticles and 18.74% for platelet nanoparticles when the thermal radiation parameter values fall between 0 to 2.5.

5. Conclusions

This study aimed to investigate the influence of thermal radiation, Cattaneo-Christov heat flux, couple stress, and shape factor on the flow of tangent hyperbolic hybrid nanofluid through a nonlinear stretching sheet. The primary objective is to understand how these parameters affect the fluid velocity and temperature profiles, and irreversibility analysis. Outcomes are displayed for two kinds of nanoparticles i.e., spherical shaped and platelet shaped. Key findings are presented below:

- A higher volume proportion of graphene oxide nanoparticles is associated with an increasing heat transmission rate.

- Rise in Weissenberg number causes a decrement in the fluid velocity.
- It has been found that a stronger magnetic field (because of the Lorentz force) and more nanoparticles (because of more friction) slow down the flow of fluid. On the other hand, a larger couple stress parameter speeds up the flow by removing obstacles.
- It is detected that the thermal radiation directly influences temperature, with higher values leading to a significant rise and a longer thermal relaxation time allowing for slower thermal transfer, resulting in a decrease in temperature.
- It is noticed that the rise in couple stress parameter causes an increment in the entropy generation but decreases the Bejan number.
- For both cases, the friction factor increases by 7.69% as the couple stress parameter value falls between 0.5 and 3.
- The rate of heat transfer rises by 19.83% for spherical nanoparticles and 18.74% for platelet nanoparticles when the thermal radiation parameter values fall between 0 to 2.5.

Future Scope

- Investigate the effects of slip and jump boundary conditions at the surface, which can be relevant in micro/nano-scale applications.
- Consider more complex nanofluid models, such as those incorporating Brownian motion, thermophoresis, and variable thermophysical properties.
- Employ machine learning algorithms to predict and optimize the behaviour of nanofluid flows based on simulation results.

Nomenclature

u, v - Velocity components in x, y directions	δ - Thermal relaxation time
n - Power lax index	Γ - Thermal relaxation parameter (non- dimensional)
μ - Dynamic viscosity	We - Weissenberg number
ρ - Density	Cs - Couple stress parameter
Υ - Positive time constant	Ra - Thermal radiation parameter
σ^* - Stefan-Boltzmann Constant	Bi - Biot number
k^* - Mean absorption Coefficient	Br - Brinkman number
k - Thermal conductivity	α - Temperature difference Parameter
γ_0 - Coefficient of couple Stress	h_f - Convective heat transfer coefficient
C_p - Specific heat of the Fluid	

References

[1] O. Pourmehran, M. Rahimi-Gorji, and D. D. Ganji, "Heat transfer and flow analysis of nanofluid flow induced by a stretching sheet in the presence of an external magnetic field," *J. Taiwan Inst. Chem. Eng.*, vol. 65, pp. 162–171 (2016), doi: 10.1016/j.jtice.2016.04.035.

[2] A. A. Afify, "The influence of slip boundary condition on Casson nanofluid flow over a stretching sheet in the presence of viscous dissipation and chemical reaction," *Math. Probl. Eng.*, vol. 2017, no. 1, Article ID 3804751 (2017), doi: 10.1155/2017/3804751.

[3] G. S. Seth, A. Bhattacharyya, R. Kumar, and A. J. Chamkha, "Entropy generation in hydromagnetic nanofluid flow over a non-linear stretching sheet with Navier's velocity slip and convective heat transfer," *Phys. Fluids*, vol. 30, no. 12 (2018), doi: 10.1063/1.5054099.

[4] G. Rasool, A. Shafiq, C. M. Khalique, and T. Zhang, "Magnetohydrodynamic Darcy–Forchheimer nanofluid flow over a nonlinear stretching sheet," *Phys. Scr.*, vol. 94, no. 10, pp. 105221 (2019), doi: 10.1088/1402-4896/ab18c8.

[5] S. Misra and G. Kamatam, "Effect of magnetic field, heat generation and absorption on nanofluid flow over a nonlinear stretching sheet," *Beilstein J. Nanotechnol.*, vol. 11, no. 1, pp. 976–990 (2020), doi: 10.3762/bjnano.11.82.

[6] R. Naveen Kumar, S. Suresha, R. P. Gowda, S. B. Megalamani, and B. C. Prasannakumara, "Exploring the impact of magnetic dipole on the radiative nanofluid flow over a stretching sheet by means of KKL model," *Pramana*, vol. 95, no. 4, pp. 180 (2021), doi: 10.1007/s12043-021-02212-y.

[7] K. A. Khan, M. F. Javed, M. A. Ullah, and M. B. Riaz, "Heat and mass transport analysis for Williamson MHD nanofluid flow over a stretched sheet," *Results Phys.*, vol. 53, pp. 106873 (2023), doi: 10.1016/j.rinp.2023.106873.

[8] M. Jawad, N. Sadiq, and M. R. Ali, "Analysis of chemical reactive tangent hyperbolic nanofluid flow with Joule heating and motile microorganisms through stretchable surface," *BioNanoScience*, vol. 14, no. 2, pp. 605–618 (2024), doi: 10.1007/s12668-023-01268-x.

[9] S. A. A. Shah, N. A. Ahammad, E. M. T. E. Din, F. Gamaoun, A. U. Awan, and B. Ali, "Bio-convection effects on prandtl hybrid nanofluid flow with chemical reaction and motile microorganism over a

stretching sheet," *Nanomaterials*, vol. 12, no. 13, pp. 2174 (2022), doi: 10.3390/nano12132174.

[10] U. Farooq, M. Tahir, H. Waqas, T. Muhammad, A. Alshehri, and M. Imran, "Investigation of 3D flow of magnetized hybrid nanofluid with heat source/sink over a stretching sheet," *Sci. Rep.*, vol. 12, no. 1, pp. 12254 (2022), doi: 10.1038/s41598-022-15658-w.

[11] P. M. Patil, B. Goudar, and M. A. Sheremet, "Tangent hyperbolic ternary hybrid nanofluid flow over a rough-yawed cylinder due to impulsive motion," *J. Taibah Univ. Sci.*, vol. 17, no. 1, pp. 2199664 (2023), doi: 10.1080/16583655.2023.2199664.

[12] C. M. Mohana and B. Rushi Kumar, "Shape effects of Darcy–Forchheimer unsteady three-dimensional CdTe-C/H_2O hybrid nanofluid flow over a stretching sheet with convective heat transfer," *Phys. Fluids*, vol. 35, no. 9 (2023), doi: 10.1063/5.0168503.

[13] Z. H. Khan, W. A. Khan, S. M. Ibrahim, K. Swain, and Z. Huang, "Impact of multiple slips and thermal radiation on heat and mass transfer in MHD Maxwell hybrid nanofluid flow over porous stretching sheet," *Case Stud. Therm. Eng.*, vol. 61, pp. 104906 (2024), doi: 10.1016/j.csite.2024.104906.

[14] B. Venkateswarlu, S. Chavan, P. V. S. Narayana, and S. W. Joo, "A numerical investigation of cross-diffusion on magnetohydrodynamic Cu–Al_2O_3/H_2O hybrid nanofluid flow over a stretching sheet with chemical reaction," *Asia-Pac. J. Chem. Eng.*, vol. 19, no. 1, pp. e2985 (2024), doi: 10.1002/apj.2985.

[15] W. Jamshed and A. Aziz, "Cattaneo–Christov based study of TiO_2–CuO/EG Casson hybrid nanofluid flow over a stretching surface with entropy generation," *Appl. Nanoscience*, vol. 8, no. 4, pp. 685–698 (2018), doi: 10.1007/s13204-018-0820-y.

[16] A. Mahdy, "Entropy generation of tangent hyperbolic nanofluid flow past a stretched permeable cylinder: variable wall temperature," *Proc. Inst. Mech. Eng. Part E: J. Process Mech. Eng.*, vol. 233, no. 3, pp. 570–580 (2019), doi: 10.1177/0954408918774898.

[17] H. Hanif, I. Khan, and S. Shafie, "Heat transfer exaggeration and entropy analysis in magneto-hybrid nanofluid flow over a vertical cone: a numerical study," *J. Therm. Anal. Calorim.*, vol. 141, no. 5, pp. 2001–2017 (2020), doi: 10.1007/s10973-020-09256-z.

[18] M. A. Alazwari, N. H. Abu-Hamdeh, and M. Goodarzi, "Entropy optimization of first-grade viscoelastic nanofluid flow over a stretching sheet by using classical Keller-box scheme," *Mathematics*, vol. 9, no. 20, pp. 2563 (2021), doi: 10.3390/math9202563.

[19] J. Kayalvizhi and A. G. Vijaya Kumar, "Entropy analysis of EMHD hybrid nanofluid stagnation point flow over a porous stretching sheet with melting heat transfer in the presence of thermal radiation," *Energies*, vol. 15, no. 21, pp. 8317 (2022), doi: 10.3390/en15218317.

[20] U. Farooq, H. Waqas, M. S. Aldhabani, N. Fatima, A. Alhushaybari, M. R. Ali, and T. Muhammad, "Modeling and computational framework of radiative hybrid nanofluid configured by a stretching surface subject to entropy generation: Using Keller box scheme," *Arab. J. Chem.*, vol. 16, no. 4, pp. 104628 (2023), doi: 10.1016/j.arabjc.2023.104628.

[21] I. Sakthi, R. Das, and P. B. A. Reddy, "Entropy generation on MHD flow of second-grade hybrid nanofluid flow over a converging/diverging channel: an application in hyperthermia therapeutic aspects," *Eur. Phys. J. Spec. Top.*, vol. 233, no. 6, pp. 1233–1249 (2024), doi: 10.1140/epjs/s11734-023-00947-w.

[22] K. Sakkaravarthi and P. Bala Anki Reddy, "Non-linear thermal radiation and entropy generation on MHD Casson and Williamson hybrid nanofluids across a curved stretching sheet with Cattaneo–Christov heat flux model," *Radiat. Eff. Defects Solids*, vol. 179, no. 3–4, pp. 386–420 (2024), doi: 10.1080/10420150.2023.2283840.

[23] I. Ahmed, M. Alghamdi, M. Amjad, F. Aziz, T. Akbar, and T. Muhammad, "Numerical investigation of MHD flow of hyperbolic tangent nanofluid over a non-linear stretching sheet," *Heliyon*, vol. 9, no. 7, pp. e17658 (2023), doi: 10.1016/j.heliyon.2023.e17658.

[24] T. Salahuddin and M. Awais, "Cattaneo–Christov flow analysis of unsteady couple stress fluid with variable fluid properties: By using Adam's method," *Alex. Eng. J.*, vol. 81, pp. 64–86 (2023), doi: 10.1016/j.aej.2023.09.021.

[25] E. A. Algehyne, A. Al-Bossly, F. S. Alduais, M. Y. Almusawa, and A. Saeed, "Significance of the inclined magnetic field on the water-based hybrid nanofluid flow over a nonlinear stretching sheet," *Nanotechnology*, vol. 34, no. 21, pp. 215401 (2023), doi: 10.1088/1361-6528/acbda1.

[26] P. Prashar and O. Ojjela, "Numerical investigation of ZnO–MWCNTs/ethylene glycol hybrid nanofluid flow with activation energy," *Indian*

J. Phys., vol. 96, no. 7, pp. 2079–2092 (2022), doi: 10.1007/s12648-021-02132-y.

[27] N. S. Akbar, A. Ebaid, and Z. H. Khan, "Numerical analysis of magnetic field effects on Eyring–Powell fluid flow towards a stretching sheet," *J. Magn. Magn. Mater.*, vol. 382, pp. 355–358 (2015), doi: 10.1016/j.jmmm.2015.01.088.

[28] A. M. Amer, S. A. Al Rashdi, N. I. Ghoneim, and A. M. Megahed, "Tangent hyperbolic nanofluid flowing over a stretching sheet through a porous medium with the inclusion of magnetohydrodynamic and slip impact," *Results Eng.*, vol. 19, pp. 101370 (2023), doi: 10.1016/j.rineng.2023.101370.

Received December, 2024